

Over half of the far-infrared background light comes from galaxies at $z \geq 1.2$

Mark J. Devlin¹, Peter A. R. Ade², Itziar Aretxaga³, James J. Bock⁴, Edward L. Chapin⁵, Matthew Griffin², Joshua O. Gundersen⁶, Mark Halpern⁵, Peter C. Hargrave², David H. Hughes³, Jeff Klein¹, Gaalen Marsden⁵, Peter G. Martin^{7,8}, Philip Mauskopf², Lorenzo Moncelsi², Calvin B. Netterfield^{8,9}, Henry Ngo⁵, Luca Olmi^{10,11}, Enzo Pascale², Guillaume Patanchon¹², Marie Rex¹, Douglas Scott⁵, Christopher Semisch¹, Nicholas Thomas⁶, Matthew D. P. Truch¹, Carole Tucker², Gregory S. Tucker¹³, Marco P. Viero⁸ & Donald V. Wiebe⁹

Submillimetre surveys during the past decade have discovered a population of luminous, high-redshift, dusty starburst galaxies^{1–8}. In the redshift range $1 \leq z \leq 4$, these massive submillimetre galaxies go through a phase characterized by optically obscured star formation at rates several hundred times that in the local Universe. Half of the starlight from this highly energetic process is absorbed and thermally re-radiated by clouds of dust at temperatures near 30 K with spectral energy distributions peaking at 100 μm in the rest frame⁹. At $1 \leq z \leq 4$, the peak is redshifted to wavelengths between 200 and 500 μm . The cumulative effect of these galaxies is to yield extragalactic optical and far-infrared backgrounds with approximately equal energy densities. Since the initial detection of the far-infrared background (FIRB)¹⁰, higher-resolution experiments have sought to decompose this integrated radiation into the contributions from individual galaxies. Here we report the results of an extragalactic survey at 250, 350 and 500 μm . Combining our results at 500 μm with those at 24 μm , we determine that all of the FIRB comes from individual galaxies, with galaxies at $z \geq 1.2$ accounting for 70% of it. As expected, at the longest wavelengths the signal is dominated by ultraluminous galaxies at $z > 1$.

The Balloon-borne Large-Aperture Submillimeter Telescope (BLAST) was designed as a precursor to the Spectral and Photometric Imaging Receiver (SPIRE) instrument^{11,12} on the European Space Agency's Herschel Space Observatory. BLAST samples the emission from galaxies at 250, 350 and 500 μm close to the peak of the FIRB. The multiwavelength observations of BLAST fill the wavelength gap between the Multiband Imaging Photometer on NASA's Spitzer satellite (MIPS; 24–160 μm) and the windows at 850 μm and 1.2 mm accessible from the ground, providing a more complete understanding of galaxy evolution at this formative epoch.

The BLAST cosmological survey of the Great Observatories Origins Deep Survey¹³ (GOODS-South) region combines a wide-area map of 8.7 square degrees with a deeper, confusion-limited map of 0.8 square degrees. These nested surveys, which are the focus of this paper, are hereafter known as the BGS-Wide and BGS-Deep observations, respectively. The depth of the BGS-Deep map was chosen to produce maps that have high signal-to-noise ratios and in which the fluctuations are dominated by pixel-to-pixel fluctuations in signals from galaxies rather than detector noise. The BLAST map (Fig. 1) overlaps

some of the deepest multiwavelength data that exist in a cosmological survey, including radio, infrared, optical (Hubble Ultra Deep Field) and X-ray (Extended Chandra Deep Field-South) surveys^{13,14}. The

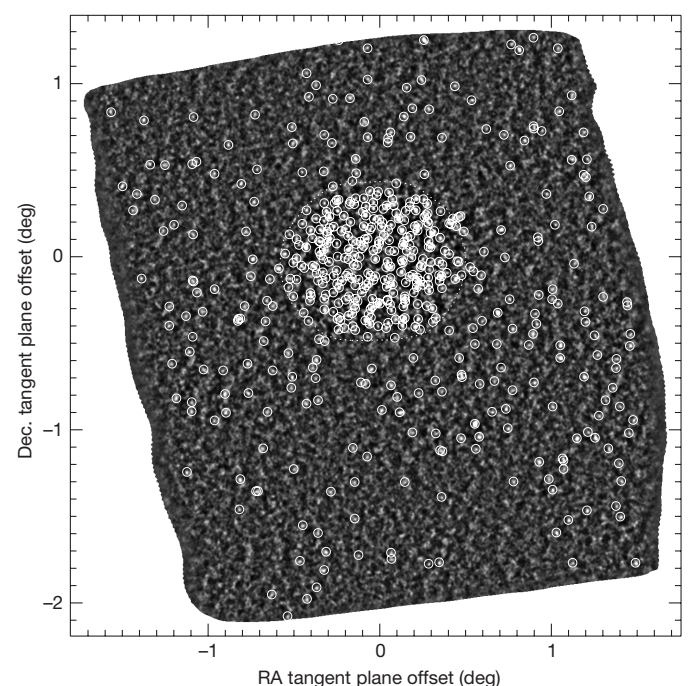


Figure 1 | Map showing the signal-to-noise ratio combination of all three BLAST bands for the entire BLAST GOODS-South observation. The circles show the locations of the ~ 500 sources extracted from the map that are detected with a signal-to-noise ratio > 5 . The 0.8-square-degree BGS-Deep region, centred at right ascension (RA) 3 h 32 min 28 s, declination (dec.) $-27^\circ 48' 30.00''$ was mapped to 1σ depths of 11, 9 and 6 mJy at 250, 350 and 500 μm , respectively, and contains 253 sources. It is visible as the region of high density in detected sources in the map. The 8.7-square-degree BGS-Wide field was mapped to 1σ depths of 36, 31 and 20 mJy at 250, 350 and 500 μm , respectively, and contains 261 sources. A more detailed description of the map making is provided in Supplementary Information.

¹Department of Physics & Astronomy, University of Pennsylvania, 209 South 33rd Street, Philadelphia, Pennsylvania 19104, USA. ²School of Physics & Astronomy, Cardiff University, 5 The Parade, Cardiff CF24 3AA, UK. ³Instituto Nacional de Astrofísica Óptica y Electrónica, Aptdo. Postal 51 y 72000 Puebla, Mexico. ⁴Jet Propulsion Laboratory, Pasadena, California 91109-8099, USA. ⁵Department of Physics & Astronomy, University of British Columbia, 6224 Agricultural Road, Vancouver, British Columbia V6T 1Z1, Canada. ⁶Department of Physics, University of Miami, 1320 Campo Sano Drive, Coral Gables, Florida 33146, USA. ⁷Canadian Institute for Theoretical Astrophysics, University of Toronto, 60 St George Street, Toronto, Ontario M5S 3H8, Canada. ⁸Department of Astronomy & Astrophysics, University of Toronto, 50 St George Street, Toronto, Ontario M5S 3H4, Canada. ⁹Department of Physics, University of Toronto, 60 St George Street, Toronto, Ontario M5S 1A7, Canada. ¹⁰University of Puerto Rico, Rio Piedras Campus, Physics Department, Box 23343, UPR Station 00931, Puerto Rico. ¹¹INAF – Osservatorio Astrofisico di Arcetri, Largo E. Fermi 5, I-50125 Firenze, Italy. ¹²Université Paris Diderot, Laboratoire APC, 10 rue Alice Domon et Léonie Duquet, 75205 Paris, France. ¹³Department of Physics, Brown University, 182 Hope Street, Providence, Rhode Island 02912, USA.

BGS-Wide map was designed to match the coverage area and sensitivity of the near-infrared and mid-infrared Spitzer Wide-area Infrared Extragalactic survey¹⁵. By considering both of the data sets together, we derive a catalogue of sources that covers a large dynamic range, (a factor of 50 in flux density) with sufficient sensitivity to resolve the FIRB into individual galaxies. The area is large enough that the source counts are minimally affected by clustering. The BLAST survey contains approximately 500 sources with significant ($>5\sigma$) detections.

The brightness distribution, or number counts, of submillimetre sources probes the luminosity function in relation to redshift and can be used to constrain models for the formation and evolution of dusty, star-forming galaxies. Models that simultaneously fit the entire range of existing data (24–850 μm) include at least two distinct galaxy populations with different spectral energy distributions and evolutionary histories^{16,17}. The BLAST data uniquely bridge these wavelengths across the energetic peak in the FIRB, and provide new strong constraints on the details of the evolution of these populations.

The number counts cannot be obtained directly from the distribution of detected sources in the BLAST catalogues because of several well-known biases. (1) The steep decrease in the counts with increasing flux density results in an Eddington bias whereby many more faint sources are boosted, rather than diminished in brightness, by noise fluctuations¹⁸. (2) The completeness of the survey falls off steeply at the faint end of the catalogue. (3) Multiple faint sources blend into brighter sources owing to a high surface density of the weakest sources and the 30–60'' resolution of the BLAST experiment. Rather than attempting to correct our source list for each of these effects, we estimate the counts from the distribution of pixel brightnesses in the entire map. This $P(D)$ analysis¹⁹ implicitly handles all of the effects mentioned above, yet uses more of the information available to us than just the brightest pixels of the extracted point sources in our catalogues.

Figure 2 shows the BLAST number counts with the results from experiments spanning 24–850 μm , for comparison. The BLAST counts are consistent with a single power law at low flux density. We can place limits on the shape of the number counts at the faint end by comparison with the FIRB. Using the naive model that the power law continues down to some limiting flux S_0 , with no sources fainter than S_0 , we find that the inferred integrated surface brightness equals the FIRB when $S_0 = 7.0 \pm 1.3$, 7.2 ± 1.7 and 4.6 ± 1.2 mJy at 250, 350 and 500 μm , respectively. A break in the counts, to a shallower slope, must occur at flux densities higher than the above limits to ensure that the integrated signal from the BLAST surveys is consistent with the amplitude of the FIRB. The increased sensitivity and higher resolution of SPIRE¹¹ should enable deeper surveys to detect the location of this spectral break.

BLAST is insensitive to individual sources significantly fainter than the 'confusion limit', which is conventionally defined as the flux at which sources reach a surface density of one object per 40 beams¹⁹. The confusion limits for BLAST and estimates of those for SPIRE based on the BLAST number counts are given in Table 1. We note that, through the $P(D)$ analysis, BLAST is sensitive to the number counts well below the confusion limit.

A stacking analysis using known positions of sources selected at different wavelengths is a powerful tool to estimate the contribution of a class of objects to the background at the wavelength of a particular map. The average brightness of these objects is calculated as the mean flux density measured at all of the positions in the map, a procedure that detects signals well below the threshold in signal-to-noise ratio used to make the BLAST catalogue. The contribution to the background from any stacked population is the product of its mean flux density and its surface density. A more detailed description of this method is provided in Supplementary Information.

We stack the 24- μm Far-Infrared Deep Extragalactic Legacy (FIDEL) survey catalogue (M. E. Dickinson *et al.*, in preparation) against the BLAST maps. The FIDEL catalogue contains sources

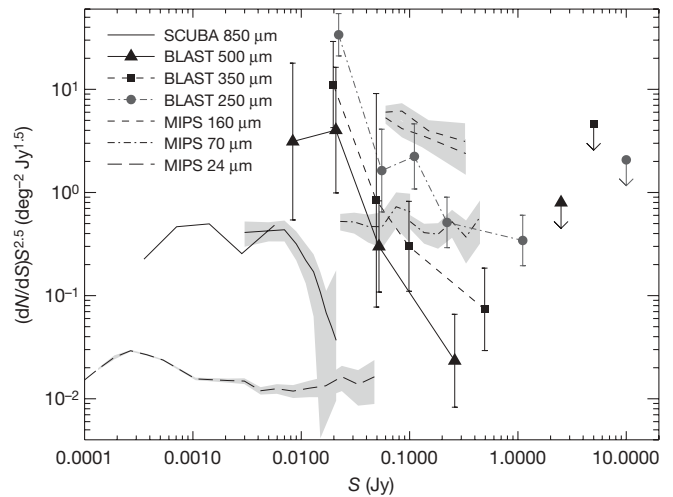


Figure 2 | The differential source counts at a variety of submillimetre and far-infrared wavelengths. If there is no evolution in number density or luminosity, we expect number counts to be Euclidean with $dN/dS \propto S^{-2.5}$. We have therefore multiplied the counts by $S^{2.5}$ so that a Euclidean slope would be horizontal. The BLAST 250, 350 and 500- μm counts (circles, squares and triangles) are measured by $P(D)$ analysis, as described in the text and Supplementary Information. Other data shown (lines only) are SCUBA 850- μm counts^{5,27} (solid lines); MIPS 160- μm counts²⁸ (short-dashed lines); MIPS 70- μm counts²⁸ (dash-dot lines); MIPS 24- μm counts²⁰ (long-dashed lines). The error bars are 1σ ; the shaded regions are 1σ error bands; the upper limits are 2σ . Nearby sources, such as the brighter sources measured at 24 μm , appear Euclidean. The counts at 850 μm are steep, which is an indication of strong evolution. A striking feature of the BLAST counts is that the slope steepens with increasing wavelength: this is the transition from the short-wavelength part of the FIRB dominated by local sources to the longer-wavelength regime dominated by distant starburst galaxies. There appears to be a break in the 500- μm counts at the low end. However, the large error bar in the last bin and the fact that adjacent bins are inherently anti-correlated make the result not very significant.

brighter than 13 mJy. The stacked flux values are given in Table 2. We include a ~ 7 –10% correction for completeness of the FIDEL catalogue based on extrapolation of 24- μm counts²⁰. From the results of these calculations, shown in Table 2, we conclude that the FIDEL sources produce 75–100% of the FIRB as measured using the Far-Infrared Absolute Spectrophotometer (FIRAS)²¹ on NASA's Cosmic Background Explorer.

Results similar to those from BLAST have been reported by stacking 24- μm Spitzer sources against the 70- μm and 160- μm maps²². Those data, recorded at wavelengths shorter than the peak intensity of the spectral energy distribution, are biased towards the low-redshift ($z \lesssim 1$) population that contributes to the FIRB. Surveys at 850 μm using the Submillimetre Common-User Bolometer Array (SCUBA) at the James Clerk Maxwell Telescope (Mauna Kea, Hawaii) sampled the higher-redshift contribution but resolved only 20–30% of the FIRB above the confusion limit⁵. Techniques using gravitational lensing to identify fainter sources below the confusion limits of ground-based submillimetre telescopes have been claimed to resolve a larger fraction

Table 1 | Source confusion limits determined by BLAST

Wavelength (μm)	BLAST r.m.s. flux density from sources (mJy)	BLAST confusion flux density (mJy)	SPIRE confusion flux density (mJy)
250	18	33 ± 4	22 ± 2
350	13	30 ± 7	22 ± 4
500	12	27 ± 4	18 ± 5

The fluctuations in the BLAST maps result from a combination of instrument noise and signals from sources. For each of the BLAST bands listed in the first column, the second column gives the residual map fluctuations from sources after subtracting instrument noise. The third and fourth columns give the formal confusion limits for BLAST and for SPIRE based on BLAST $P(D)$ analysis and the respective beam sizes. The confusion limit is the source brightness, S_{conf} , for which there is one source for every 40 beams. r.m.s., root mean squared.

Table 2 | The results of the 24- μm stacked flux

Wavelength (μm)	Stacked flux ($\text{nW m}^{-2} \text{sr}^{-1}$)	Corrected flux ($\text{nW m}^{-2} \text{sr}^{-1}$)	FIRB ($\text{nW m}^{-2} \text{sr}^{-1}$)
250	7.9 ± 0.5	8.5 ± 0.6	10.4 ± 2.3
350	4.5 ± 0.3	4.8 ± 0.3	5.4 ± 1.6
500	2.0 ± 0.2	2.2 ± 0.2	2.4 ± 0.6

For each of the BLAST bands in the first column, the second and third columns give the stacked and completeness-corrected fluxes, respectively. The fourth column is the expected flux determined by FIRAS²¹. The precision of the astrometry is 5". To verify the astrometry, the stacked flux was shown to drop off in all directions when the map is shifted with respect to the 24- μm catalogue. A similar stack was made against the 2-Ms Chandra Deep Field-South survey catalogue²⁵ which resolves $\sim 80\%$ of the soft and hard X-ray backgrounds²⁶. We find that these sources account for about 14% of the FIRB. Because active galactic nuclei account for 55% of the sources in the Chandra catalogue²⁵, we conclude that they only comprise 7% of the FIRB, although there may be a small contribution from Compton-thick active galactic nuclei that is missed.

of the FIRB²³. The wide spectral coverage of the BLAST data allows us to probe the Universe at both low redshift and high redshift. To demonstrate this, we use the Spitzer Infrared Array Camera (IRAC) colours to broadly divide the FIDEL catalogue into different populations to examine their relative contributions to the background at BLAST wavelengths. Using sources of known redshift in the GOODS Multiwavelength Southern Infrared Catalogue²⁴, we were able to define a simple cut in IRAC colours that effectively divides the catalogue into two galaxy populations above and below $z = 1.2$. At 250 μm , we find that there are approximately equal contributions to the background from sources above and below $z = 1.2$. We also note a systematic increase to 55% at 350 μm and 70% at 500 μm in the proportion of the background produced by sources at $z > 1.2$. These results are consistent with our expectation that objects in the longer-wavelength BLAST channels are dominated by the ultraluminous $z > 1$ galaxies discovered by SCUBA at 850 μm .

BLAST is the first instrument to make confusion-limited maps of the sky at wavelengths near the peak of the FIRB with enough sensitivity, sky coverage and angular resolution to identify a large number of sources, determine the detailed shape of the source counts and show that most of the FIRB comes from submillimetre sources already identified in deep 24- μm surveys. Combining these data with the results at 70 and 160 μm , we can account for essentially all of the FIRB with known galaxies. Combining the BLAST and future Herschel data at 250, 350 and 500 μm with spectroscopic and photometric redshifts will allow a determination of the optically obscured star-formation history of the Universe. These data will also provide catalogues of luminous submillimetre sources that will benefit from high-resolution imaging and spectroscopy from the Atacama Large Millimetre/submillimetre Array as we improve our understanding of galaxy formation and evolution in the high-redshift Universe.

Received 19 November 2008; accepted 9 February 2009.

1. Smail, I., Ivison, R. J. & Blain, A. W. A deep sub-millimetre survey of lensing clusters: a new window on galaxy formation and evolution. *Astrophys. J.* **490**, L5–L9 (1997).
2. Hughes, D. H. *et al.* High-redshift star formation in the Hubble Deep Field revealed by a submillimetre-wavelength survey. *Nature* **394**, 241–247 (1998).
3. Barger, A. J. *et al.* Submillimetre-wavelength detection of dusty star-forming galaxies at high redshift. *Nature* **394**, 248–251 (1998).
4. Greve, T. R. *et al.* A 1200- μm MAMBO survey of ELAIS2 and the Lockman Hole - I. Maps, sources and number counts. *Mon. Not. R. Astron. Soc.* **354**, 779–797 (2004).

5. Coppin, K. *et al.* The SCUBA Half-Degree Extragalactic Survey - II. Submillimetre maps, catalogue and number counts. *Mon. Not. R. Astron. Soc.* **372**, 1621–1652 (2006).
6. Eales, S. *et al.* The Canada-UK Deep Submillimetre Survey. IV. The survey of the 14 hour field. *Astron. J.* **120**, 2244–2268 (2000).
7. Borys, C., Chapman, S., Halpern, M. & Scott, D. The Hubble Deep Field North SCUBA Super-map - I. Submillimetre maps, sources and number counts. *Mon. Not. R. Astron. Soc.* **344**, 385–398 (2003).
8. Laurent, G. T. *et al.* The Bolocam Lockman Hole Millimeter-Wave Galaxy Survey: galaxy candidates and number counts. *Astrophys. J.* **623**, 742–762 (2005).
9. Coppin, K. *et al.* The SCUBA Half Degree Extragalactic Survey - VI. 350- μm mapping of submillimetre galaxies. *Mon. Not. R. Astron. Soc.* **384**, 1597–1610 (2008).
10. Puget, J.-L. *et al.* Tentative detection of a cosmic far-infrared background with COBE. *Astron. Astrophys.* **308**, L5–L8 (1996).
11. Griffin, M. *et al.* The Herschel-SPIRE instrument and its capabilities for extragalactic astronomy. *Adv. Space Res.* **40**, 612–619 (2007).
12. Pascale, E. *et al.* The Balloon-borne Large Aperture Submillimetre Telescope: BLAST. *Astrophys. J.* **681**, 400–414 (2008).
13. Giavalisco, M. *et al.* The Great Observatories Origins Deep Survey: initial results from optical and near-infrared imaging. *Astrophys. J.* **600**, L93–L98 (2004).
14. Lehmer, B. D. *et al.* The Extended Chandra Deep Field-South Survey: Chandra point-source catalogs. *Astrophys. J. Suppl. Ser.* **161**, 21–40 (2005).
15. Lonsdale, C. J. *et al.* SWIRE: The SIRTf Wide-Area Infrared Extragalactic Survey. *Publ. Astron. Soc. Pacif.* **115**, 897–927 (2003).
16. Lagache, G. *et al.* Polycyclic aromatic hydrocarbon contribution to the infrared output energy of the Universe at $z \approx 2$. *Astrophys. J. Suppl. Ser.* **154**, 112–117 (2004).
17. Rowan-Robinson, M. The star formation history of the Universe: an infrared perspective. *Astrophys. J.* **549**, 745–758 (2001).
18. Eddington, A. S. The correction of statistics for accidental error. *Mon. Not. R. Astron. Soc.* **100**, 354–361 (1940).
19. Condon, J. J. Confusion and flux-density error distributions. *Astrophys. J.* **188**, 279–286 (1974).
20. Papovich, C. *et al.* The 24 micron source counts in deep Spitzer Space Telescope surveys. *Astrophys. J. Suppl. Ser.* **154**, 70–74 (2004).
21. Fixsen, D. J., Dwek, E., Mather, J. C., Bennett, C. L. & Shafer, R. A. The spectrum of the extragalactic far-infrared background from the COBE FIRAS observations. *Astrophys. J.* **508**, 123–128 (1998).
22. Dole, H. *et al.* The cosmic infrared background resolved by Spitzer. Contributions of midinfrared galaxies to the far-infrared background. *Astron. Astrophys.* **451**, 417–429 (2006).
23. Knudsen, K. K., van der Werf, P. P. & Kneib, J.-P. Probing the submillimetre number counts at $f_{850\mu\text{m}} < 2 \text{ mJy}$. *Mon. Not. R. Astron. Soc.* **384**, 1611–1626 (2008).
24. Grazian, A. *et al.* The GOODS-MUSIC sample: a multicolour catalog of near-IR selected galaxies in the GOODS-South field. *Astron. Astrophys.* **449**, 951–968 (2006).
25. Luo, B. *et al.* The Chandra Deep Field-South Survey: 2 ms source catalogs. *Astrophys. J. Suppl. Ser.* **179**, 19–36 (2008).
26. Hickox, R. C. & Markevitch, M. Absolute measurement of the unresolved cosmic X-ray background in the 0.5–8 keV band with Chandra. *Astrophys. J.* **645**, 95–114 (2006).
27. Smail, I., Ivison, R. J., Blain, A. W. & Kneib, J.-P. The nature of faint submillimetre-selected galaxies. *Mon. Not. R. Astron. Soc.* **331**, 495–520 (2002).
28. Dole, H. *et al.* Far-infrared source counts at 70 and 160 microns in Spitzer deep surveys. *Astrophys. J. Suppl. Ser.* **154**, 87–92 (2004).

Supplementary Information is linked to the online version of the paper at www.nature.com/nature.

Acknowledgements We acknowledge the support of NASA, the US National Science Foundation Office of Polar Programs, the Canadian Space Agency, the Natural Sciences and Engineering Research Council of Canada and the UK Science and Technology Facilities Council. We are grateful to B. Magnelli for help with the FIDEL 24- μm data. This research was enabled by the WestGrid computing resources and the SIMBAD and NASA/IPAC databases. We thank the Columbia Scientific Balloon Facility, Ken Borek Air Ltd and the mountaineers of McMurdo Station for their work.

Author Information Reprints and permissions information is available at www.nature.com/reprints. Correspondence and requests for materials should be addressed to M.J.D. (devlin@physics.upenn.edu).